metals

MDPI

Article

Modular Finite Element Modeling of Heavy Plate Rolling Processes Using Customized Model Reduction Approaches

Andreas W. Nemetz [1,*], Erik Parteder [2], Paula Reimer [3], Thomas Kaltenbrunner [2], Bodo Heise [2], Jagoba Lekue [3], Thomas Gross [3], Stefan Falkner [2], Rupert Egger [2] and Klaus Zeman [1]

[1] Institute of Mechatronic Design and Production, Johannes Kepler University (JKU) Linz, Altenberger Straße 69, 4040 Linz, Austria
[2] Voestalpine Grobblech GmbH, voestalpine Straße 3, 4020 Linz, Austria; bodo.heise@voestalpine.com (B.H.)
[3] LCM–Linz Center of Mechatronics GmbH, Altenberger Straße 69, 4040 Linz, Austria; jagoba.lekue@lcm.at (J.L.)
* Correspondence: andreas_walter.nemetz@jku.at

Abstract: Heavy plates are indispensable semi-finished products. Quality is strongly linked with production, so the rolling process must be performed within well-defined narrow tolerances. To meet this challenge, adequate modeling has become a necessity. In contrast to continuous strip rolling, where the workpiece can be modeled as a semi-infinite strip and 2D modeling can be argued quite well, this strategy is insufficient for the comprehensive modeling of heavy plate rolling. The geometry of the heavy plate favors an inhomogeneous distribution of relevant state variables, such as temperature. In addition, if the process involves longitudinal and spreading passes, the required plate rotation spoils the assumption of a symmetric arrangement that might have been acceptable before rotation. Consequently, the derivation of suitably reduced models is not trivial, and modeling tailored to the specific objective of investigation is of utmost importance. Models intended to resolve the evolution of inhomogeneities in the field variables are demanding and computationally expensive. An effective modular modeling strategy was developed for such models to be used offline. Mutually complementing and interchangeable modules may constitute an efficient modeling strategy valid for the specific subject of interest. The presented approach reduces the enormous cost of complete 3D simulation as much as the model purpose allows for.

Keywords: heavy plate rolling; metal forming; plasticity; finite element method; re-meshing; model reduction; modular modeling; temperature field

Citation: Nemetz, A.W.; Parteder, E.; Reimer, P.; Kaltenbrunner, T.; Heise, B.; Lekue, J.; Gross, T.; Falkner, S.; Egger, R.; Zeman, K. Modular Finite Element Modeling of Heavy Plate Rolling Processes Using Customized Model Reduction Approaches. *Metals* **2024**, *14*, 444. https://doi.org/10.3390/met14040444

Academic Editors: Carlos Agelet de Saracibar, Michele Chiumenti, Djordje Peric and Eduardo De Souza Neto

Received: 28 February 2024
Revised: 5 April 2024
Accepted: 9 April 2024
Published: 11 April 2024

1. Introduction

Heavy plates are semi-finished products that are indispensable for industry. In addition to the quantity, the quality of the products plays a crucial role. Since constant compliance with quality requirements is becoming increasingly important, the manufacturing process, which includes the rolling process, must be performed within narrow tolerances. This narrow tolerance band requires monitoring and precise control of the process. Monitoring, in turn, requires models that enable one to interpret measurement data from the process correctly.

Online models are now standard for process support, control, and correction. They have to be powerful, considering their essential requirements of being fast. Regardless of this, such online models need verification and require field data for their validation and further development. On the one hand, data can come from the process. On the other hand, as it is just typical for metal forming processes, one is faced with the difficulty that the utmost relevant state variables, such as the time-dependent field of temperatures, strains, and stresses inside the heavy plate currently being processed, are metrologically inaccessible [1]. One is limited to signals representing estimates of the surface temperature and integral variables, such as rolling force and torque. These metrological difficulties

substantiate modeling and offline simulation using physics-based, validated models as an indispensable alternative for gaining knowledge about the heavy plate hot rolling process.

Modeling and simulation have been well-established for decades in the realm of research and development of rolling technologies. Models and methods have evolved within this period as they naturally build on one another, at least partly. The respective literature is extensive, and for this reason, a complete presentation is not feasible. Instead, only a few significant milestones, essential in the context of the presented new modular modeling approach, are chronologically listed here. A more comprehensive overview is given, for instance, in [2,3]. Additionally, aspects of current progress are briefly discussed in order to understand how the present work is embedded in the overall context.

Building on basic modeling approaches [4–6], a 2D finite element (FE) model was developed in the parametric form in 1999, in which the geometry of the work rolls and the plate in conjunction with the loads and boundary conditions are the main variables [7]. In 2004, a 3D FE model capable of simulating a steady-state rolling process was published [8]. Five years later, the crack closing behavior was modeled within a 2D FE approach [9]. In 2012, a 2D FE model was utilized to recalculate flow stresses for heavy plates from industrial process data [10]. In 2021, a 3D FE model that predicts zones within the plate with a higher fracture probability, depending on changes in relevant thermo-physical properties, was presented [11]. A review of the latest literature reveals that, on the one hand, work is currently underway to improve material models for forming processes. An in-depth, model-supported investigation of recrystallization during hot deformation associated with heavy plate rolling of C-Mn steel, Nb micro-alloyed or not, is provided in [12]. Microstructural changes in the material related to hot rolling and crucial for defining flow curves and hardening/softening effects are discussed in [13–15]. On the other hand, alternatives to conventional or variants of hot rolling processes are also being modeled and simulated. An interesting approach is a process presented as "Hot Core Heavy Reduction Rolling", the properties of which are discussed in [16–19] based on numerical and analytical studies and experimental data. In addition to simulating void healing in heavy plates, by deploying FE and phase-field simulation [20], the hot rolling of clad plates has also received increased attention recently, as numerical and experimental work shows [21–23]. Despite these achievements, one aspect still needs to be reflected: the existing models focus on individual passes rather than on the assembly of whole rolling schedules. A holistic model that covers the efficient, application-oriented simulation of the thermo-physical behavior of the plate along whole rolling schedules has not been detected. A 3D modular FE approach for the purpose of tracking the fillet of a heavy plate throughout a longitudinal rolling process consisting of several passes was published in 2023 [24]. The benefit of the modular modeling strategy shown in [24] is its ability to investigate the temperature distribution across the plate's width direction.

The model introduced in the present article is an advancement of this modular modeling strategy [24]. Integrating new routines into the model allows for the comprehensive simulation of a heavy plate rolling process, including both longitudinal and spreading passes. The associated increase in complexity and the consumption of computing time are countered with modular model reduction. Among other merits, the reduction potential is primarily exploited by on-demand utilization or rejection of different symmetries and by process state-dependent mesh generation and manipulation algorithms. An additional process of state-dependent local mesh adjustment enables the simulation of rolling schedules employing a single and modular, and thus adaptable, model.

2. Modular Modeling and Virtual Process Route

To evaluate the temperature evolution in a heavy plate throughout an entire rolling process, a sequence of FE models has been developed with which the corresponding simulations can be carried out. Such simulations support process understanding because, on the one hand, the spatial and temporal distribution of the state variables inside a heavy

plate is de facto inaccessible by measurement technologies, and, on the other hand, usual online models do not have sufficient modeling depth to provide this service.

For the automated accomplishment of central tasks, an object-orientated Python 3.8 script was developed. The script creates parameterized Abaqus/Standard 2019 and Abaqus/Explicit 2019 FE input files, which build on one another. Kinematic, mechanical–technological, and process data are taken from the rolling schedule, the material characteristics of the plate, and the plant and process specifications. The Python 3.8 script slices the model of the heavy plate hot rolling process into sub-processes and manages the sub-simulations. They will be executed one after another, and the final state (e.g., fields of displacements, stresses, and strains) of one sub-process model is transferred as an initial state to the model of the subsequent sub-process. The preparation and merging of the results from sub-simulations are performed in the Python 3.8 script as well.

The core of the Python 3.8 script is a user-defined class that represents the blueprint for an FE input file. Instances of FE input files fundamentally differ in the attributes specified in the class. A closer look at a heavy plate hot rolling (sub-)process helps to understand the purpose of the defined class's attributes.

When the slab leaves the furnace, it is first fed to the roll stand on the roller table. To a good approximation, there is a purely thermal load on the slab at the roller table since the hot slab cools down in the air. As the slab passes through the roll stand, in addition to the propagating energy exchange in the form of heat, deformation and reshaping of the rolling stock occur. From then on, the rolling stock is no longer referred to as a slab but as a plate. After the plate has left the roll stand, it is taken over again by the roller table, and the process becomes, to a good approximation, purely thermal again [24]. From this consideration, the class's first essential attribute ("load case attribute") follows to define the type of load case (thermal/thermo-mechanical). Due to the two possible values of the "load case attribute," there are initially two variants of instances of the FE input file. One is suitable for modeling the transport of the slab or plate on the roller table, and the other is employed for modeling the (thermo-mechanical) forming in the roll gap.

A key differentiating feature of the heavy plate hot rolling process compared to hot strip rolling is the possibility of rotating the rolling stock on the roller table. The rolling schedule often includes such a rotation of the plate by 90°. In these cases, in addition to the longitudinal passes, a few spreading passes are carried out in order to adjust the plate's width to a value that guarantees the final width of the plate after rolling. Afterwards, the plate is turned back to its original orientation. Suppose the rolling process includes no rotations; a symmetric model could be used to simulate the process [24]. Then, in the sense of model reduction, only the right or the left half of the system is modeled. With the idealized assumption that the rolls are perfectly rigid cylinders arranged in parallel and that the plate ideally enters the roll gap, this modeling approach can be implemented without any loss of information. The mentioned utilization describes left–right symmetry (from now on referred to as vertical symmetry). This results in a second essential attribute of the class, namely, the "symmetry attribute." If, as in most published models [10,24–26], it is assumed that the (heavy plate) rolling process meets a good approximation of top–bottom symmetry (from now on referred to as horizontal symmetry), activating the horizontal symmetry plane in the model is expedient. Four modeling variants result from combining the consideration or rejection of horizontal and vertical symmetry.

The two attributes mentioned, whereby the "load case attribute" can assume two (thermal/thermo-mechanical) and the "symmetry attribute" can take four states (no/vertical/horizontal/horizontal and horizontal symmetry), result in a total variety of eight types of input files, as seen in Figure 1. These eight model variants (from now on referred to as simulation modules), together with the initialization, intermediate control, (re)meshing, rotation, and evaluation routines (from now on referred to as interaction modules), form the different stages of a virtual process route that have been designed for efficient modeling and simulation of the overall heavy plate rolling process.

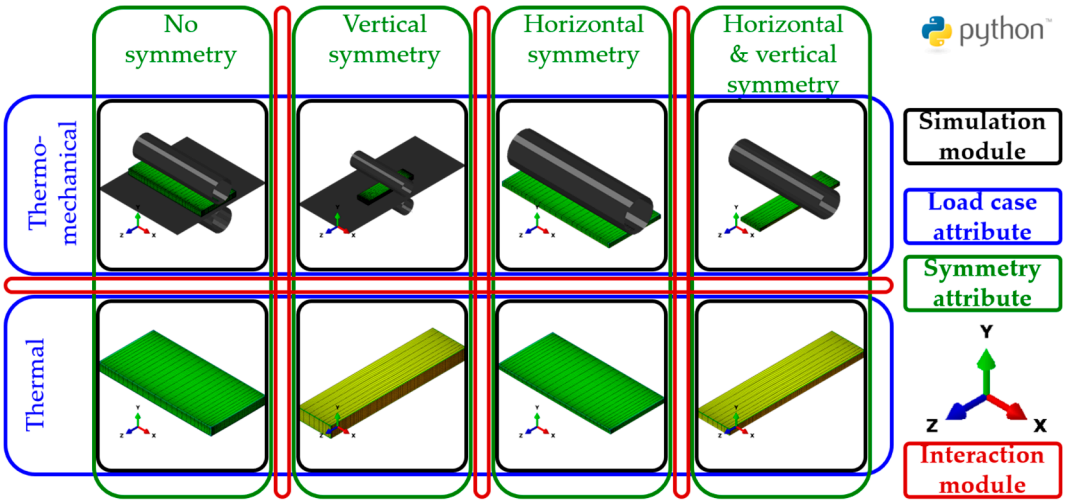

Figure 1. Matrix of the available simulation modules, depending on two attributes and the combination of their values. The simulation modules are the main building blocks of the virtual process route and are connected by interaction modules to model and simulate the rolling schedule offline.

In conclusion, the current modeling strategy offers the benefit of automatically creating efficient simulation modules, including their connection toward an optimized holistic model adapted to the underlying rolling schedule. The optimization within the modeling strategy is essential due to the computationally intensive 3D simulation and is indispensable for evaluating the time-dependent fields of state variables inside the heavy plate. The following subsections comprehensively reveal the structure and performance of the simulation and interaction modules.

2.1. Simulation Modules

As depicted in Figure 1, the "load case attribute" can take on two values (thermal/thermo-mechanical). If the value "thermal" is assigned to it, the consequence is that the slab or plate is modeled exclusively subjected to its heat exchange with the ambient air. The influence of an optionally used descaling unit on the temperature field in the plate is considered in this model variant as well. The thermo-physical data that this module requires for a valid thermal simulation are mass density, specific heat capacity, and thermal conductivity. Radiation and convection are active on the surface of the slab or plate. The Python 3.8 script takes the constant emissivity, convection, and air temperature from the process data to be provided, which determines the heat transfer from the slab or plate to the environment (and vice versa). An adapted (increased) convection allows for including optional descaling processes.

However, if the attribute is "thermo-mechanical", the model considers both the plate's thermal and mechanical interaction with the work rolls. This makes modeling of the roll stand necessary, as seen in Figure 1. In addition to the thermo-physical data mentioned above, this model requires a flow curve, Young's modulus, and Poisson's ratio of the material of the stock to be rolled. Depending on the modeling depth, these values can be functions of state variables, such as temperature. In the current model, rigid work rolls modeled by analytical cylinder surfaces with a constant temperature represent the roll stand. The penalty method modifies contact between the plate and the work roll. Normal contact is designed as "hard contact"; the tangential contact force directly results from the coefficient of friction. A shear stress limit can optionally be used [24]. The heat transfer coefficient (HTC) between the work roll and the plate, which is assumed to lie within the range of 3000 W/m^2K [22] and 24,000 W/m^2K [26], has to be provided [27]. A total of 90% of the friction work is estimated to be transformed into heat. The frictional heat generated within the mechanical contact is assumed to be transferred equally into the two friction partners. The inelastic heat fraction is considered to be 90% [28]. Section 3.1

discloses material, thermo-physical, tribological, and process data. These data correspond to the use case discussed in Section 3. Inhomogeneities in mechanical and thermal contact and accompanying effects are not explicitly considered in this holistic 3D model. The representation of these and other locally impacting aspects is currently outside the intent of this model.

Because of efficiency, the used element types depend on the "load case attribute". When modeling the thermal load case, the element type DC3D8 is employed, and when modeling the thermo-mechanical load case, the element type C3D8RT is applied. Both element types are eight-node continuum brick elements, whereby the DC3D8 elements only have temperature degrees of freedom. In contrast, the C3D8RT elements also carry thermally coupled translational displacement degrees of freedom, with reduced integration being used.

As depicted in Figure 1, the "symmetry attribute" can take four values (no/vertical/horizontal/vertical and horizontal symmetry). Depending on whether one or more symmetries may be assumed in the model of a sub-process, suiting displacement and heat flow boundary conditions on the symmetry planes of the slab or plate are employed to replace the omitted parts of the model. A possible model reduction using vertical symmetry results from the actual process state, but whether the process should be assumed to have horizontal symmetry is a matter for the user to decide.

2.2. Interaction Modules

As a first step, the parameterized simulation modules must be initialized. Secondly, state variables have to be transferred from one sub-simulation to the subsequent sub-model. Assigning values to the mesh parameters is an essential part of the initialization at the beginning of the simulation routine. The mesh generator, embedded in the interaction module, creates a regular mesh for discretizing the slab. In terms of model reduction, the aim is to reduce the number of required elements. Following this principle, biasing the mesh is included in the mesh generator to achieve finer discretization near the slab's or plate's free surfaces, where high gradients of state variables (particularly temperature) are to be expected. Parameters that control the structure of the initial mesh are the base element edge length and three bias factors (one in each edge direction of the cuboid slab). Since the material flow is predominant in the rolling direction and the contact patch moves longitudinally, rolling direction-dependent meshing is implemented in the model. Except for the edge zones, the discretization in the current width direction is coarsened by a factor of four. The structure of the slab's initial mesh is shown in Figure 2. On the one hand, the length and width bias factors refer to a local coordinate system linked with the plate. Hence, a rotation of the plate does not affect this material-fixed assignment. On the other hand, a rotation of the plate changes the orientation of the rolling direction; therefore, the former coarse-meshed direction turns to the fine-meshed direction and vice versa. Mesh refinement demands the generation of intermediate nodes, including a linear interpolation of coordinates and temperatures at these nodes. Mesh coarsening requires the deletion of nodes and the fusion of elements.

In addition to generating the (initial) mesh, an integrated sequential mesh adaptation is crucial to the prospect of success of the modeling strategy. An automated, stable simulation of an entire rolling schedule is only possible with this intervention. The change in the shape of the plate driven by the material flow requires the mesh to be adapted to the process. To keep the element aspect ratio within specified limits, the elongation and spreading of the plate are taken into account by on-demand mesh refinements in the longitudinal and width directions. The thickness reduction is compensated by coarsening the mesh. This mesh adaptation is deliberately kept simple. When refining the mesh in the longitudinal or width direction, intermediate nodes are inserted in the corresponding direction, doubling the number of elements along this direction. When coarsening the mesh in the thickness direction, every second node is removed, and the number of elements in this direction is halved. This means that the coarser mesh is contained in the finer mesh, and the

elements' compatibility is guaranteed, as seen in Figure 3a. In addition, this strategy makes interpolation routines for the state variables obsolete when transferring them from the original to the adapted mesh.

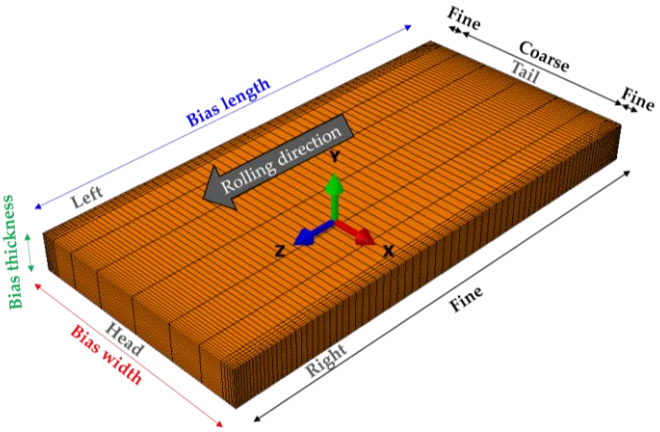

Figure 2. Structure of the initial mesh of the slab considering developing temperature gradients at the free surfaces, the material flow, pronounced in the rolling direction, and a moving contact patch. Due to regular meshing, potential symmetry planes are equipped with nodes to be constrained by boundary conditions. In the case of prevailing symmetry, these boundary conditions substitute redundant areas of the plate (not shown in this figure). The convention for using the terms head, tail, left, and right within this article is outlined.

However, this method cannot ensure a stable simulation along the entire heavy plate rolling process when used alone. Since parts of the vertical surfaces of the slab are transformed into horizontal surfaces of the plate due to the reduction in thickness and the associated material flow at the edges, the elements that discretize this area may degenerate during the forming process. Hence, automated node adjustment is performed in the corresponding mesh areas to prevent the degeneration of affected elements. Considering a cross-section of the plate, one can see that the edge is represented by a triple of nodes (node -1, node 0, and node 1). These nodes, shown schematically in Figure 3b, are identified in the first step. The interior angle α between the two vectors that point from node 0 to node 1 and node -1, respectively, is then calculated in the second step. If α is less than 150°, this geometry segment is interpreted as an edge. If this angle criterion is violated, the edge has moved to a neighboring node. This edge migration requires the nodes to be adjusted to maintain mesh quality. In step three, node 0 assumes the position and temperature of node 1 and is now called node 0*. Node 1 is moved to a position midway between nodes 0* and 2 and is renamed node 1*. The temperature at node 1* is linearly interpolated accordingly. This procedure is outlined in Figure 3b. After completing this elementary adjustment, nodes 1* and 2 to n, nodes -5 to -1 will be arranged evenly on the side and the top (or bottom) surface, with the temperature at the adjusted nodes being adapted using linear interpolation. n is the number of nodes along the side surface's upper (or bottom) half, reduced by 1. This adjustment of the nodes on the edges recovers the mesh structure on the plate's free surfaces near the edge.

However, this manipulation potentially disrupts the regularity of the elements in the bulk. For this reason, an adjustment mechanism is installed downstream. Degenerate elements are identified and rehabilitated using an angle criterion. Suppose the angle β between two element edges of the examined element is outside the tolerable range of 30° to 150°. In this case, the node located at the vertex is slightly moved to bring the angle back into the fair range. The temperature at such nodes is interpolated accordingly. An abstraction of this procedure is outlined in Figure 3c.

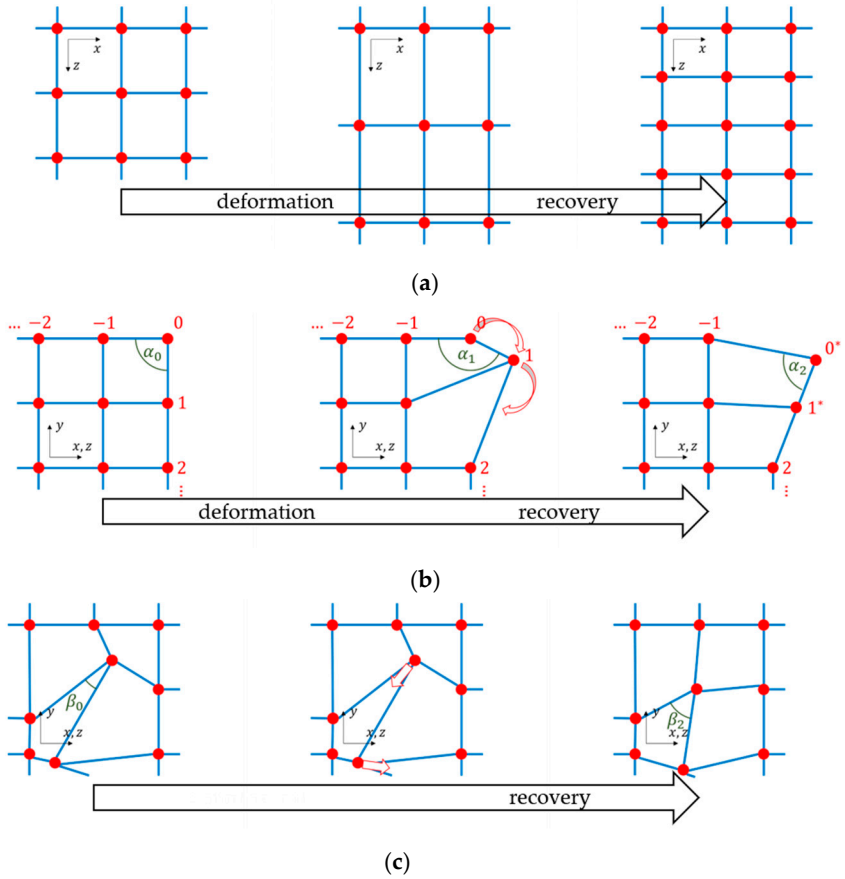

Figure 3. Mesh adaptation. (**a**) The increase in length of the plate associated with rolling leads to a stretch of the elements in the rolling direction with a simultaneous compression in the thickness direction. During the rolling process, which consists of several passes, the ratio of the lengths of the element edges is evolving adversely. The ratio is improved by inserting nodes along the stretched direction, simultaneously dividing each element into two ones. The inverse method is applied in the compressed direction by removing nodes, which leads to a union of two superimposed elements into one element in the thickness direction. (**b**) The migration of edges leads to a degeneration of the elements at these edges. This negative effect is eliminated by a systematic rearrangement and adjustment of the nodes on the surface in the edge area, and degenerated elements recover. (**c**) Due to the high deformation, combined with the necessary mesh adaptation at the edges, the regularity of the mesh inside the bulk may be disturbed. Elements degenerated in this way are identified using an angle criterion and repaired by slightly moving affected nodes.

In the current state of development, the simulation requires the specification of a homogeneous initial slab temperature and a constant work roll temperature. The angular velocity of the work rolls and the corresponding initial velocity of the plate are adapted for each pass from the rolling schedule or the process data. The plate geometry and the underlying mesh at the end of each sub-simulation are transferred to be the initial geometry and mesh of the subsequent sub-model, onto which the temperature is mapped. In addition, manipulations such as rotating the plate and the associated evaluation of existing symmetries must be carried out in conjunction with the rolling schedule. Any misalignments of the plate that may occur [29] are automatically corrected within the interaction module when the geometry is transferred from the current sub-simulation to the subsequent sub-model.

3. Application, Correlation with Measured Process Data, and Discussion

The performance of the modeling strategy is demonstrated by investigating a use case. Considering the available rolling schedule, shown in Table 1, and the configuration of the

roll stand and the slab, the model is supplied with material, thermo-physical, and tribological data to simulate the loading history of a heavy plate from leaving the furnace to the last pass. The assumption of horizontal symmetry was made because the model is validated via the top surface temperature of the plate, one of the few available data measured on the plant at specific times (passes 1, 3, 6, 18, 19, and 20) during the rolling process.

Table 1. Data from the rolling schedule.

Pass	Time [s]	Plate Velocity [mm/s]	Plate Thickness after Pass [mm]	Measured Fillet Surface Temperature [°C]
1	69	718	255	1091
2	88	2012	242	-
3	140	1885	215	1040
4	148	1938	187	-
5	155	1961	158	-
6	164	716	134	1043
7	184	2195	130	-
8	189	2225	128	-
9	196	2196	127	-
10	691	2480	114	-
11	699	2367	106	-
12	707	2396	99	-
13	715	2184	92	-
14	724	2172	86	-
15	732	2141	80	-
16	741	2151	74	-
17	750	2150	68	-
18	759	2147	62	880
19	768	2145	57	875
20	778	3044	51	882

Additionally, in Section 3.3, results from simulations of this rolling schedule are shown, in which the assumption of horizontal symmetry is spoiled, and an adapted convection is applied to the bottom plate surface. This parameter is intended to provide the model's capability to roughly estimate the roller table's thermal influence on developing an asymmetric temperature field. This simulation should be viewed as a numerical experiment, as validation is, at this stage, impossible due to a lack of metrologically accessible data in the investigated industrial process. Still, validation is being attempted via laboratory experiments. The roller table is modeled rudimentarily by a rigid surface on which the plate is supported vertically and slides without friction. The vertical position of the modeled roller table, not perfectly aligned to the pass line but with a 20 mm offset, together with the actual slab or plate thickness, significantly affects the kinematic conditions at the roll gap entry.

Figure 4 shows the virtual process route condensed from the rolling schedule to be simulated, as outlined in Table 1. An essential feature of the rolling schedule under consideration is that the plate is rotated after the first and after the sixth pass. Hence, five spreading passes are carried out.

The presented study focuses on a reliable calculation of the heavy plate's process- and material-dependent temperature development. The possibility of displaying all results of interest was considered in the model's design so that the temporal evaluation of any material point inside the plate and on its surface is possible. Post-processing is decoupled from simulation. This means that it can also be applied to existing simulation results generated with this model. Hence, if the focus of the research question changes, a quick response may be possible.

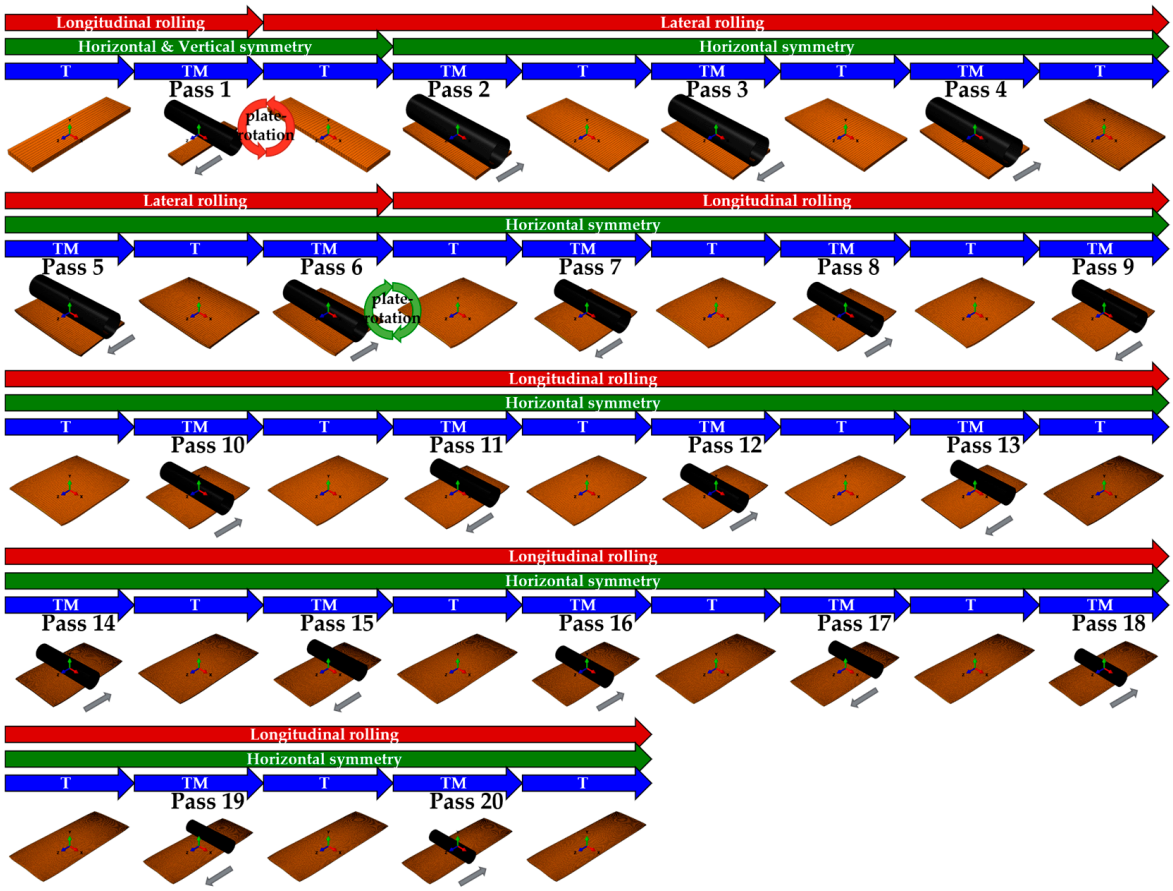

Figure 4. The automatically built virtual process route corresponds to the given rolling schedule. The plate is rotated after the first pass. This rotation spoils the symmetry of the process. Therefore, the value of the "symmetry attribute" changes accordingly. The change in the "load case attribute" is clearly outlined by the alternating sequence of modeling types "thermal (T)" and "thermo-mechanical (ITM)", respectively.

In the temperature assessment, the position on the top of the fillet of the slab serves as a reference, as this temperature may be available for validation. Additional references at this fillet position are the numerically evaluated temperatures at the quarter-thickness and the plate's core. Four further positions (material fixed in the thickness direction) included in the investigation are offset equidistantly inwards in the longitudinal direction from the slab's head, as seen in Figure 2. The total offset amount corresponds to 400 mm on the rolled plate (after the last pass). This offset was chosen because it needs to be examined whether the temperature gradient in the longitudinal direction has decayed sufficiently and, hence, a sample taken from this position is representative of the rolled heavy plate in terms of its material properties. In other words, the model can be used to predict and, hence, minimize the crop lengths at the heavy plate's head and tail ends that have to be cut off as scrap since these parts might violate specified temperature ranges during rolling. Accordingly, the position this material point initially had on the slab can be retraced based on the deformation history of the plate. Table 2 lists the positions measured from the head surface that are dependent on elongation.

Table 2. List of positions at which the temperature's temporal evolution is evaluated compared to the reference temperature in the fillet.

Pass	Plate Length after Pass [mm]	Actual Offset from the Head Surface			
		Position 1 [mm]	Position 2 [mm]	Position 3 [mm]	Position 4 [mm]
slab	3460	36	71	107	142
1	3686	38	76	114	152
2	1794	18	37	55	74
3	2022	21	42	62	83
4	2327	24	48	72	96
5	2741	28	56	85	113
6	3225	33	66	99	133
7	3824	39	79	118	157
8	3897	40	80	120	160
9	3913	40	80	121	161
10	4353	45	90	134	179
11	4694	48	97	145	193
12	5012	52	103	155	206
13	5371	55	110	166	221
14	5763	59	118	178	237
15	6199	64	127	191	255
16	6700	69	138	207	276
17	7288	75	150	225	300
18	7970	82	164	246	328
19	8766	90	180	270	360
20	9727	100	200	300	400

3.1. Material, Thermo-Physical, and Tribological Data Utilized in the Use Case

The processed plate consists of tempered steel with 0.088 m-% C and 1.510 m-% Mn. An elasto-plastic formulation describes the material behavior of the plate. The elastic behavior is determined by the two material parameters: temperature-dependent Young's modulus, depicted in Figure 5a, and Poisson's ratio of 0.3.

Beyond the yield limit, the material is deforming plastically with 90% of the plastic energy as heat sources. Individual and temperature- and strain-dependent flow stress curves are selected for each pass, based on the mean strain rate in the deformation zone of each individual pass, to approximate the microstructural dynamics during plastification [13–15]. As an example, the temperature- and strain-dependent flow curves of passes 9 and 20 are shown in Figure 5b. Due to high rolling temperatures, it can be estimated that the material is fully recrystallized after each pass. Hence, an undeformed initial state is assumed immediately before each pass. If this is not the case, more sophisticated material models are necessary to achieve satisfactory accuracy. The modular model is open to any material model supported by Abaqus/Explicit 2019.

The thermo-physical quantities of specific heat and heat conductivity are assumed to be functions of temperature. As depicted in Figure 5c,d, these two values are linearized within the considered temperature ranges. The mass density is supposed to be constant at 7837 kg/m^3.

The heat transfer coefficient for air convection is 12 W/m^2K, except for the descaling phases, where it takes a value of 2000 W/m^2K. In both cases, the associated water or air temperature is 20 °C. The emissivity coefficient is assumed to be 0.792 with an associated air temperature of 20 °C.

The Coulomb friction model is assigned a coefficient of friction of 0.5.

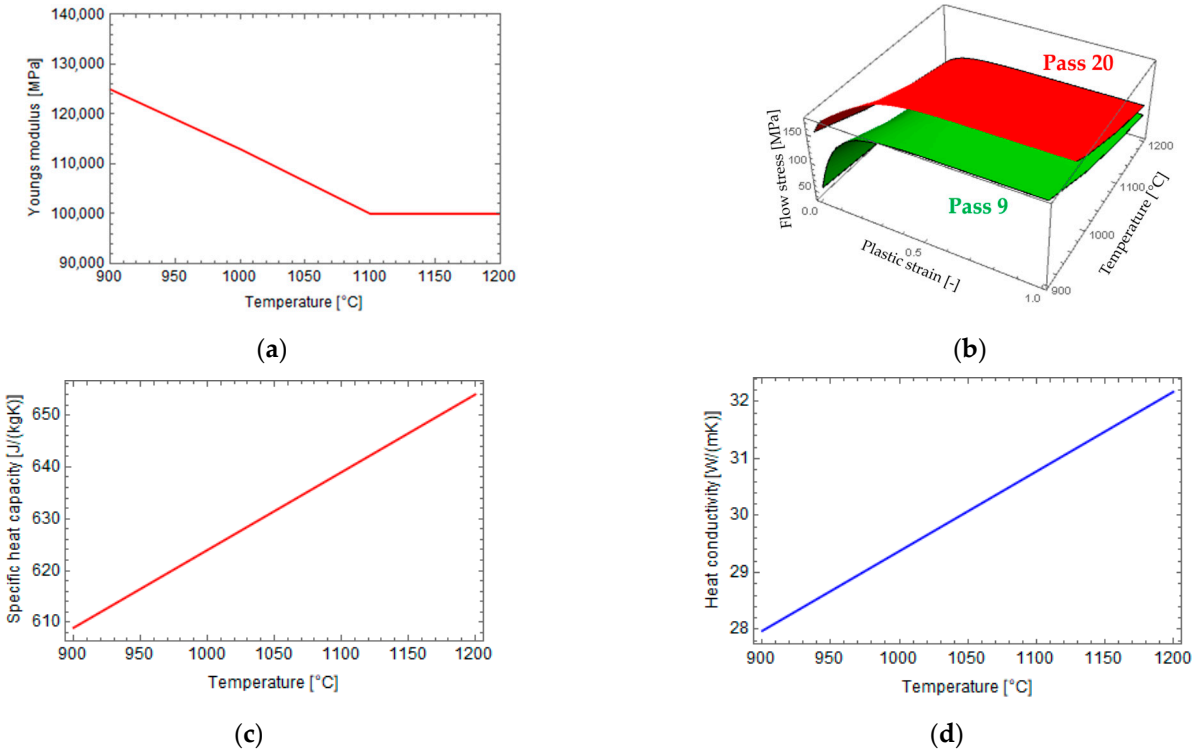

Figure 5. Material data of the heavy plate. (**a**) Young's modulus as a function of temperature, linearized; (**b**) flow curves for passes 9 and 20 as functions of temperature and strain; (**c**) specific heat capacity as a function of temperature, linearized; (**d**) heat conductivity as a function of temperature, linearized.

3.2. Evolution of Temperature

The initial configuration, prescribing the geometry and homogeneous temperature of the slab leaving the furnace, is given in Table 3. The constant diameter and temperature of the work rolls are given in this table as well. According to the virtual process route (Figure 4), the simulation starts with a thermal FE quarter model of the slab, as this model reduction can be used without loss of information due to the system's double symmetry. The assumption of horizontal symmetry is maintained throughout the entire process. Still, the vertical symmetry is disturbed and, therefore, abandoned after the rotation of the plate, immediately before the second pass.

Table 3. Initial configuration of the slab leaving the furnace and constant work roll configuration.

Slab				Work Roll	
Length [mm]	**Width [mm]**	**Thickness [mm]**	**Initial Temperature [°C]**	**Diameter [mm]**	**Temperature [°C]**
3460	1707	273	1226	1000	100

The time course of temperatures at the surface, core, and quarter-thickness positions are shown in Figure 6a. The homogeneous temperature field is disturbed immediately when the slab leaves the furnace due to thermal radiation and convection on the plate's free surfaces. When the passes are executed (Table 1), abrupt temperature drops are observed on the surface of the plate due to contact with the colder work rolls. This effect is often called the surface chilling effect [25,30]. Judging by the model, the local temperature does not drop to an extent that would impair the mechanical properties of the semi-finished product. However, due to the temperature level and the heat conduction in the plate,

reheating occurs immediately. In the process under consideration, the descaling unit is activated twice, once before the first pass and again between the second and third pass. The jets of water, sprayed onto the plate by the descaling unit, also lead to a sudden cooling of the surface, which is again quickly counterbalanced by heat conduction. The water jets, therefore, have no significant influence on the caloric temperature of the plate.

As depicted in Figure 6a, the calculated temperature at the surface of the plate matches well with the measured temperatures given in Table 1. This is especially true for the last three measurement points to which the model is tuned (in terms of radiation and convection). Hence, considering unavoidable measurement inaccuracies, the validation can be assessed positively for this model, which aims to evaluate the temperature field inside the plate.

The course of the temperature in the plate's core, depicted in Figure 6a, reveals a characteristic that is different from that of the surface temperature. At the plate's core, the effects at the surface, resulting from the heat exchange with the work rolls, the ambient air, and the water from the descaling unit, have subsided. In contrast to the surface, an increase in temperature is observed in the core due to plastic deformation during a pass. The same applies to the temperature curve, evaluated at the quarter-thickness position. Overall, the time course of the inhomogeneity of the temperature in the thickness direction can be seen from this representation (Figure 6a). The initially homogeneous temperature field becomes more and more inhomogeneous up to the ninth pass. Afterwards, the graphs show an appropriate holding time that is due to thermo-mechanical rolling in order to adjust the specified mechanical properties of the final heavy plate. This period of approximately 500 s exhibits a decrease in temperature inhomogeneities. During the last passes, temperatures are balanced more and more, largely due to the decreasing thickness of the heavy plate.

The previous discussion considered the temperature development in conjunction with the plastic deformation and the sole heat transfer from the plate's upper (and symmetrically arranged lower) free surface. This effect could also be depicted with a 2D model if the consideration is limited to the fillet [31]. However, heat flux on the plate's side surfaces must be considered to delimit the fillet from the crop in the longitudinal direction. In Figure 6b, the solid lines, therefore, show surface, core, and quarter-thickness temperatures at position 1. Comparing the temperature curves at the reference fillet position (dotted curves in Figure 6b) with that at position 1 (solid line in Figure 6b) illustrates the influence of the side surfaces. A temperature gradient in the longitudinal direction is present here. The surface, quarter-thickness, and core temperatures after the last pass at position 1 are reduced by 77 °C, 104 °C, and 127 °C compared to corresponding temperatures at the reference (fillet) position. Evaluation of the three vertical positions at position 2, shown in Figure 6c, delivers temperature drops of 38 °C, 55 °C, and 67 °C relative to the reference position. Positions 1 and 2 belong to the cut-off scrap [32]. Positions 3 and 4, shown in Figure 6d,e, have temperature differences of 20 °C, 32 °C, and 38 °C and 9 °C, 17 °C, and 22 °C, respectively. This shows that at positions 3 and 4, the influence of the head side surface (Figure 2) has almost subsided since the temperatures reach $\geq$96% of the corresponding fillet temperatures. In conclusion, forming in the vicinity of positions 3 and 4 proceeds under thermal conditions very close to those prevailing in the fillet.

In addition to the time course, the temperature profile in the longitudinal direction is relevant to assess the thermal conditions during forming. Figure 7 shows the temperature profiles after the ninth and the final pass. The areas of homogeneous temperature can easily be identified from this representation, thus indirectly indicating the potential size of the scrap that may need to be discarded.

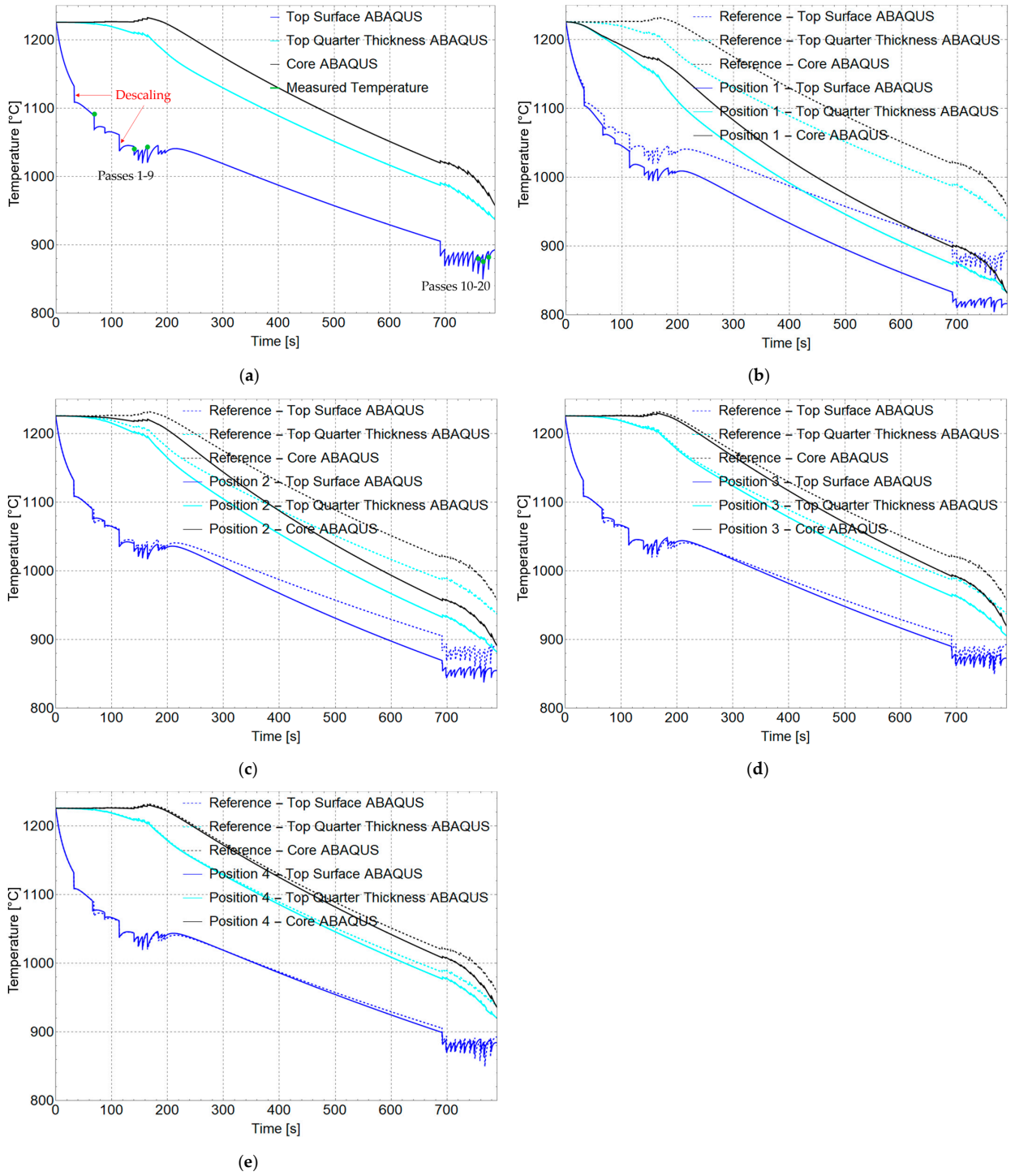

Figure 6. Temperatures as a function of time evaluated at three vertical positions in the plate. These vertical positions are the surface, the quarter-thickness, and the core position. (**a**) Validation of the temperature calculation via measured temperatures at the surface of the plate located at the fillet (reference) position. The influence of the descaling water jets is illustrated. (**b**) Temperatures at material-fixed position 1. This position belongs to the cut-off scrap. (**c**) Temperatures at material-fixed position 2. This position belongs to the cut-off scrap. (**d**) Temperatures at material-fixed position 3. (**e**) Temperatures at material-fixed position 4. The initial positions 1 to 4 and their updating distances from the head of the plate are listed in Table 2.

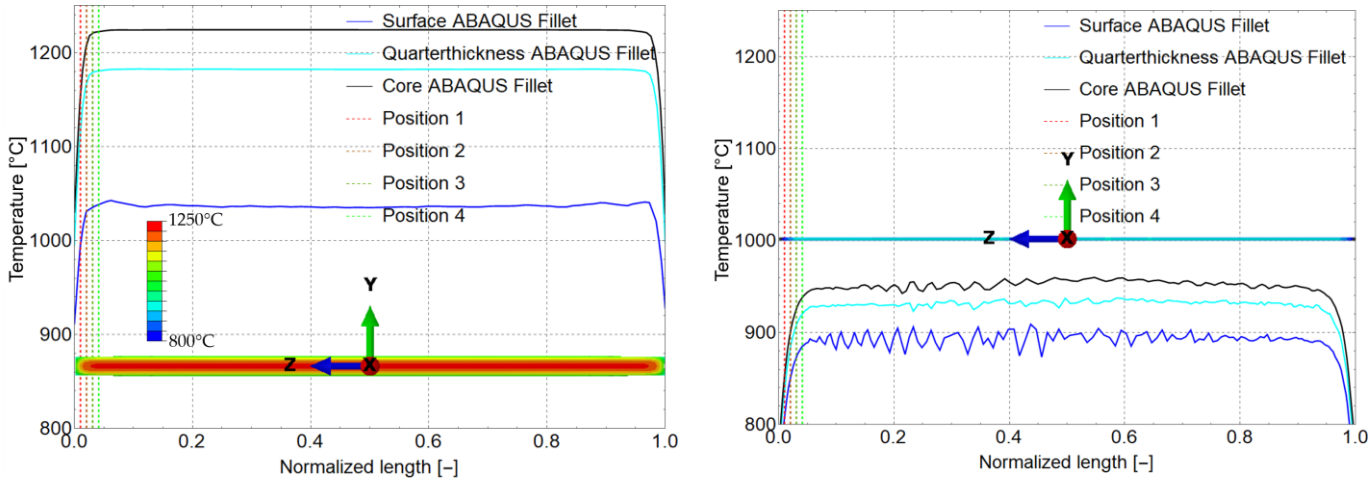

Figure 7. Temperature profiles at three vertical positions in the plate. These positions are the surface, the quarter-thickness, and the core position. Temperature profiles at the reference position (fillet) in the longitudinal direction (**a**) after the ninth pass and (**b**) after the last pass.

3.3. Thermal Asymmetry

The suggestion that a rolling process has an inherent horizontal symmetry is a usual modeling assumption because data from industrial processes showing the thermal influence of the roller table on a developing asymmetrical temperature field in the plate cannot be reliably identified at this time. However, the present modular modeling strategy (Figure 1) is able to build a horizontally asymmetric model [21–23] to initiate a theoretical investigation through adapted convection, which acts on the bottom free surface of the plate. Employment of this model may deliver an equivalent convection factor through iterative application in conjunction with reliable temperature data (also inside the plate) that may be available in the future.

In the numerical study shown here, the convection factor at the bottom of the plate was doubled, resulting in a more significant amount of heat being retracted from the bottom surface of the plate compared to the top surface. The temperature profiles after the ninth pass within the fillet on the two free surfaces (top/bottom), on the two quarter-thicknesses, and in the core are shown in Figure 8.

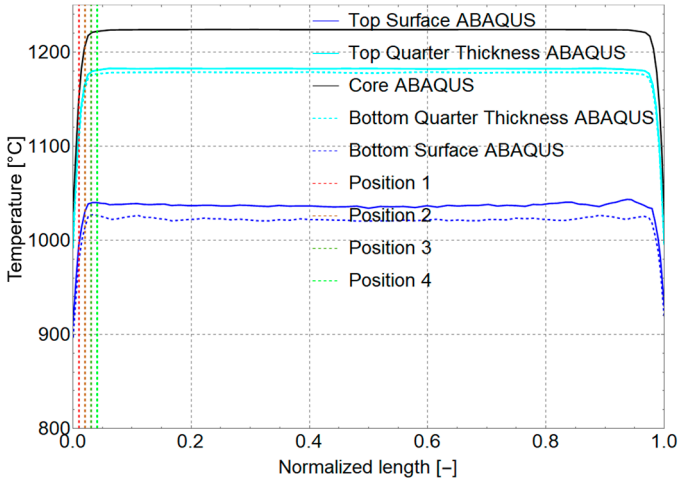

Figure 8. Longitudinal temperature profiles at five vertical positions in the plate were evaluated numerically after the ninth pass. These positions are the top surface, the top quarter-thickness, the core, the bottom quarter-thickness, and the bottom surface.

4. Conclusions and Outlook

When creating and validating models, particular attention has to be paid to the fact that any model is an abstraction of an original from a particular perspective with a specific focus. The current modeling strategy aims to reliably evaluate the temperature at any point in and on the plate during the heavy plate rolling process. As the validation shows, this has proven possible, provided the material and thermo-physical data are of sufficient quality. The chosen modeling approach represents a step towards establishing a modular model as a benchmark, augmenting existing models of any kind. Concerning the calculation of temperature fields, this seems to have largely succeeded. The model includes the effects of heat transfer at the plate's surfaces, heat conduction inside the plate, and heat generation due to plastic deformation work. It can already be used to reliably predict the temperature field not only inside the fillet part of heavy plates but also at any point of its boundaries in the length and width direction, thus offering plenty of information for the improvement and optimization of heavy plate products.

The actual focus of the presented model on temperature fields and their validation follows from the fact that attention was to be paid to interfaces to which corresponding modules still being developed can dock.

Future work will focus on the validation and reliable prediction of spatially distributed plastic strains and (residual) stresses as well, which may necessitate a somewhat finer spatial discretization. In any case, the models developed so far will serve as a foundation for the design and validation of these even more advanced models.

Author Contributions: Conceptualization, A.W.N., E.P., P.R., T.K., B.H., J.L., T.G., S.F., R.E. and K.Z.; methodology, A.W.N., E.P., T.K. and K.Z.; software, A.W.N.; validation, A.W.N., E.P., T.K. and B.H.; formal analysis, A.W.N. and K.Z.; resources, A.W.N., E.P., T.K. and B.H.; data curation, A.W.N., E.P. and T.K.; writing—original draft preparation, A.W.N. and K.Z.; writing—review and editing, E.P., P.R., T.K., B.H., J.L., T.G., S.F. and R.E.; visualization, A.W.N.; supervision, E.P., T.K. and K.Z.; project administration, A.W.N., E.P., P.R., T.K., J.L., T.G., R.E. and K.Z.; funding acquisition, T.G., R.E. and K.Z. All authors have read and agreed to the published version of the manuscript.

Funding: This research was funded by the COMET-K2 Center of the Linz Center of Mechatronics (LCM) funded by the Austrian federal government and the federal state of Upper Austria (Grant No. 886468 (FFG)). This work was supported by the Johannes Kepler Open Access Publishing Fund and the federal state of Upper Austria. Open Access Funding by the University of Linz.

Data Availability Statement: The data presented in this study are available on request from the corresponding author (privacy).

Conflicts of Interest: Authors Erik Parteder, Thomas Kaltenbrunner, Bodo Heise, Stefan Falkner and Rupert Egger were employed by the company Voestalpine Grobblech GmbH. Authors Paula Reimer, Jagoba Lekue and Thomas Gross were employed by the company LCM–Linz Center of Mechatronics GmbH. The remaining authors declare that the research was conducted in the absence of any commercial or financial relationships that could be construed as a potential conflict of interest.

References

1. Jo, S.Y.; Hong, S.; Han, H.N.; Lee, M. Modeling and Simulation of Steel Rolling with Microstructure Evolution: An Overview. *Steel Res. Int.* **2023**, *94*, 2200260. [CrossRef]
2. Rout, M.; Pal, S.K.; Singh, S.B. Finite Element Modeling of Hot Rolling: Steady- and Unsteady-State Analyses. In *Computational Methods and Production Engineering*; Davim, J.P., Ed.; Woodhead Publishing: Sawstoun, UK, 2017; pp. 83–124.
3. Mistry, G.D.; Judal, K.B. Literature review of the stress, strain and separating force evaluation during hot bar rolling of different types of steels. *Mater. Today Proc.* **2022**, *57*, 636–642. [CrossRef]
4. Sims, R.B. The calculation of roll force and torque in hot rolling mills. *Proc. Inst. Mech. Eng.* **1954**, *168*, 191. [CrossRef]
5. Maccagno, T.M.; Jonas, J.J.; Hodgson, P.D. Spreadsheet Modelling of Grain Size Evolution during Rod Rolling. *ISIJ Int.* **1996**, *36*, 720. [CrossRef]
6. Siciliano, F.; Minami, K.; Maccagno, T.M.; Jonas, J.J. Mathematical modeling of the mean flow stresses, fractional softening and grain size during the hot strip rolling of C-Mn steels. *ISIJ Int.* **1996**, *36*, 1500. [CrossRef]
7. Galantucci, L.M.; Tricarico, L. Thermo-mechanical simulation of a rolling process with an FEM approach. *J. Mater. Process. Technol.* **1999**, *92–93*, 494. [CrossRef]

8. Wisselink, H.H.; Huétink, J. 3D FEM simulation of stationary metal forming processes with applications to slitting and rolling. *J. Mater. Process. Technol.* **2004**, *148*, 328. [CrossRef]
9. Deng, W.; Zhao, D.W.; Qin, X.M.; Du, L.X.; Gao, X.H.; Wang, G.D. Simulation of central crack closing behavior during ultra-heavy plate rolling. *Comput. Mater. Sci.* **2009**, *47*, 439–447. [CrossRef]
10. Parteder, E.; Zeman, K.; Du, H.; Grill, R. Recalculation of Flow Stresses from Industrial Process Data for Heavy Plate Rolling Using a 2D Finite Element Model. *Steel Res.* **2012**, *83*, 124–130. [CrossRef]
11. González-Castillo, A.C.; Cruz-Rivera, J.d.J.; Ramos-Azpeitia, M.O.; Garnica-González, P.; Garay-Reyes, C.G.; Pacheco-Cedeño, J.S.; Hernández-Rivera, J.L. 3D-FEM Simulation of Hot Rolling Process and Characterization of the Resultant Microstructure of a Light-Weight Mn Steel. *Crystals* **2021**, *11*, 569. [CrossRef]
12. Klančnik, G.; Foder, J.; Bradaškja, B.; Kralj, M.; Klančnik, U.; Lalley, P.; Stalheim, D. Hot Deformation Behavior of C-Mn Steel with Incomplete Recrystallization during Roughing Phase with and without Nb Addition. *Metals* **2022**, *12*, 1597. [CrossRef]
13. Renault, C.; Churyumov, A.; Pozdniakov, A.V.; Churyumova, T.A. Microstructure and hot deformation behavior of FeMnAlCMo steel. *J. Mater. Res. Technol.* **2020**, *9*, 4440–4449. [CrossRef]
14. Zhou, J.; Yu, Z.; Chen, J.; Wu, S.; Wu, K.; Pan, L. The Performance of Niobium-Microalloying Ultra-High-Strength Bridge Cable Steel during Hot Rolling. *Materials* **2024**, *17*, 1259. [CrossRef] [PubMed]
15. Cui, S.; Gu, G.; Shi, C.; Xiao, G. Variations in microstructure and mechanical properties along thickness direction in a heavy high strength low alloy steel plate. *J. Mater. Res. Technol.* **2023**, *26*, 9190–9202. [CrossRef]
16. Li, H.; Li, T.; Gong, M.; Wang, Z.; Wang, G. Finite Element Analysis of Dynamic Recrystallization of Casting Slabs during Hot-Core Heavy Reduction Rolling Process. *Metals* **2020**, *10*, 181. [CrossRef]
17. Li, H.; Gong, M.; Li, T.; Wang, Z.; Wang, G. Effects of hot-core heavy reduction rolling during continuous casting on microstructures and mechanical properties of hot-rolled plates. *J. Mater. Process. Technol.* **2020**, *283*, 116708. [CrossRef]
18. Li, R.; Li, H.; Ning, X.; Li, T.; Wie, H.; Wang, G. Temperature Influence on Section Uniformity of Casting Steel Rolled with the Hot-Core Heavy Reduction Rolling Process and Traditional Hot Rolling Process. *J. Mater. Eng. Perform.* **2022**, *31*, 7391–7401. [CrossRef]
19. Li, T.; Gao, P.; Li, H.; Tang, X.; Wang, X.; Ren, J.; Wang, Z. Comparison of Dynamic Recrystallization in Blooms between Conventional Rolling and Hot-Core Heavy Reduction Rolling Process. *Steel Res.* **2023**, *94*, 2300043. [CrossRef]
20. Ning, Z.; Li, X.; Liu, H.; Cai, Q.; Yu, W. Experimental and Simulation Study on the Effect of Reduction Pretreatment on the Void Healing of Heavy Plate. *Metals* **2022**, *12*, 400. [CrossRef]
21. Liu, Y.; Li, Y.; Wang, Z.; Liu, Y.; Wang, T.; Huang, Q.; Wang, T. Deformation mechanism and microstructure evolution in stainless steel clad plate of longitudinal corrugated hot rolling. *J. Mater. Process. Technol.* **2023**, *316*, 117957. [CrossRef]
22. Cheng, Y.; Liu, W.; Wang, T.; Li, T.; Huang, Q. Study on the effects of initial temperature and thickness ratio of component metals on the preparation of aluminum/steel clad plates by the new different temperature rolling method. *J. Manuf. Process.* **2023**, *95*, 229–241. [CrossRef]
23. Guo, X.; Ren, Z.; Chai, Z.; Wang, T.; Huang, Q. Research on microstructure and mechanical properties of TC4/304 clad plates by asymmetric rolling with local strong stress. *Mater. Sci. Eng. A* **2024**, *893*, 146166. [CrossRef]
24. Nemetz, A.W.; Parteder, E.; Reimer, P.; Kaltenbrunner, T.; Heise, B.; Lekue, J.; Gross, T.; Egger, R.; Zeman, K. Towards a 2D/3D FE-Based Digital Twin for the Approximation of Metrologically Inaccessible Dynamic Fields of State Variables During Heavy Plate Rolling. *Steel Res.* **2023**, *94*, 2200672. [CrossRef]
25. Han, J.; Cheng, Q.; Hu, P.; Xing, H.; Li, S.; Ge, S.; Hua, X.; Hu, B.; Zhang, W.; Wang, K. Finite Element Analysis of Large Plastic Deformation Process of Pure Molybdenum Plate during Hot Rolling. *Metals* **2023**, *13*, 101. [CrossRef]
26. Hwang, J.-K. Thermal Behavior of a Rod during Hot Shape Rolling and Its Comparison with a Plate during Flat Rolling. *Processes* **2020**, *8*, 327. [CrossRef]
27. Li, Y.H.; Krzyzanowski, M.; Beynon, J.H.; Sellars, C.M. Physical simulation of interfacial conditions in hot forming of steels. *Acta Metall. Sin.* **2000**, *13*, 359–368.
28. Longère, P.; Dragon, A. Evaluation of the inelastic heat fraction in the context of microstructure-supported dynamic plasticity modelling. *Int. J. Eng.* **2008**, *35*, 992–999. [CrossRef]
29. Pietschnig, C.; Steinboeck, A.; Kugi, A. Optimal control of motion and camber of steel plates in a multi-pass reversing rolling process. *IFAC-PapersOnLine* **2022**, *55*, 180–185.
30. Ding, Y.; Zhu, Q.; Le, Q.; Zhang, Z.; Bao, L.; Cui, J. Analysis of temperature distribution in the hot plate rolling of Mg alloy by experiment and finite element method. *J. Mater. Process. Technol.* **2015**, *225*, 286–294. [CrossRef]
31. Lekue, J.; Reimer, P.; Parteder, E.; Nemetz, A.W.; Kaltenbrunner, T.; Heise, B.; Falkner, S.; Gross, T.; Egger, R.; Zeman, K. Characterization of thermomechanical effects in heavy plate hot rolling as a function of process settings. In Proceedings of the METEC & 6th ESTAD 2023, Düsseldorf, Germany, 12–16 June 2023.
32. Cao, J.; Wang, Y.; Huang, S.; Wang, C. Optimized shearing strategy for heavy plate based on contour recognition. *J. Iron Steel Res. Int.* **2023**, *30*, 1821–1833. [CrossRef]